Transverse Particle Trapping Using Finite Bessel Beams Based on Acoustic Metamaterials

Xudong Fan,[1,*] Yifan Zhu,[2] Zihao Su,[2] Ning Li,[1] Xiaolong Huang,[1] Yang Kang,[1] Can Li,[1] Chunsheng Weng,[1] Hui Zhang,[2,†] Weiwei Kan,[3,‡] and Badreddine Assouar[4,§]

[1] *National Key Laboratory of Transient Physics, Nanjing University of Science and Technology, Nanjing 210094, China*

[2] *Jiangsu Key Laboratory for Design and Manufacture of Micro-Nano Biomedical Instruments, School of Mechanical Engineering, Southeast University, Nanjing 211189, China*

[3] *School of Science, MIIT Key Laboratory of Semiconductor Microstructure and Quantum Sensing, Nanjing University of Science and Technology, Nanjing 210094, China*

[4] *Université de Lorraine, CNRS, Institut Jean Lamour, F-54000 Nancy, France*

(Received 31 October 2022; accepted 13 February 2023; published 9 March 2023)

We investigate the transverse trapping force acting on a small particle on or off the central axis of zero-order finite Bessel beams. Combining the simulated fields with the Gorkov force potential, the transverse trapping behaviors for small objects are analyzed, and the reversal of the trapping behaviors is recovered when varying the paraxiality parameter of the Bessel beam. The results prove the possibility of using axisymmetric Bessel beams to trap both dense and stiff particles as well as light and soft ones. The particles can be trapped at the maximum central pressure in the main lobe and also the maximum pressure of the other transverse locations. A lossy acoustic metastructure with the ability to decouple the phase and amplitude modulations is used to generate the desired sound field, which is used to trap a foam ball as an example. Our research opens a promising avenue to the design and development of simplified acoustic tweezers.

DOI: 10.1103/PhysRevApplied.19.034032

I. INTRODUCTION

Acoustic wave, as one of the most important forms in classical wave systems, plays a significant role in the development of science and technology. When an object is placed in an acoustic field, there exists an acoustic radiation force acting on it. The force originates from the momentum transfer from the field to the object due to scattering, reflection, and absorption. The acoustic radiation force acts throughout the object, but owing to the overall momentum conservation, the radiation force can be reduced to an integration of the time-averaged momentum-flux tensor over an arbitrary closed surface enclosing the whole object [1]. Acoustic radiation forces have been studied for a long time in regards to sound waves of different forms [2–17]. The trapping behaviors generated by standing waves on small objects (object sizes are much smaller than the wavelength) have been well understood [2], where relatively light and soft particles (like droplets) are trapped to the pressure maximum (antinode), yet relatively dense and stiff particles (like elastic objects) are trapped to the pressure minimum (node). On the other hand, recent studies of acoustic radiation forces based on nondiffracting beams [4–6,14,15,18–20] have predicted the possibility for particle manipulations with more flexibility. However, in practical situations and applications, nondiffracting beams, such as acoustic Bessel beams, are difficult to generate by a finite source due to relatively complex transverse structures. Hence, it is significantly important to precisely generate and control the desired sound field. The conventional method would use a speaker or transducer array connected with a multisignal generator, and then the desired sound field could be generated by adjusting the signal for each speaker or transducer individually [10]. Sound field manipulation based on such an active method has the advantage of flexibility, yet as the complexity of the array system increases, the cost and the complexity of the signal processing will also increase. Hence, it is desirable to realize precise field manipulations with simplicity and low cost. Recently, the emergence and the rapid development of acoustic metamaterials [21] have opened a field in acoustics, and also provide an approach for field manipulations [22–39]. Acoustic metamaterials can exhibit extraordinary properties and phenomena, which for natural materials would be difficult to achieve, such as

*fanxudong@njust.edu.cn
†seuzhanghui@seu.edu.cn
‡kan@njust.edu.cn
§badreddine.assouar@univ-lorraine.fr

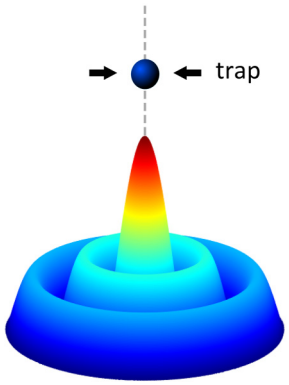

FIG. 1. Illustration of transverse particle trapping by acoustic Bessel beams.

negative refraction and/or reflection [22,23], cloaking [40–44], holograms [11,36,45–47], and specific field generations [22,24,32].

In this work, we investigate the transverse acoustic radiation force generated by finite Bessel beams based on acoustic metamaterials. The transverse trapping behaviors of a small particle on or off the central axis of the Bessel beams are studied numerically and experimentally. A lossy acoustic metastructure, capable of decoupling the phase and amplitude modulations, is designed to generate the desired Bessel field, which is then used to trap a small foam ball to the beam center as an example. Our work gives insight into some unusual and unique trapping behaviors, which will help the further study of particle manipulations using acoustic radiation forces and acoustic Bessel fields.

II. NUMERICAL SIMULATION

We consider here a particle within a finite axisymmetric Bessel beam (Fig. 1), which can be approximately considered as a nondiffracting beam within a certain transverse radius and a certain propagating distance. The pressure field within such regions Re$[p(\mathbf{r},t)]$ (Re denotes the real part) of finite zero-order Bessel beams propagating along the z axis is given by

$$p(\mathbf{r},t) = p_0 J_0(\mu\rho)\exp(i\kappa z - i\omega t), \tag{1}$$

where p_0 is a real-valued amplitude, J_0 is zero-order Bessel function, $\mathbf{r}(\rho,\phi,z)$ is the field point in cylindrical coordinates, and the transverse wavenumber μ and axial wavenumber κ are related to the total wavenumber $k = \sqrt{\mu^2+\kappa^2} = \omega/c_0$ (c_0 is the speed of sound in the surrounding media) through a paraxial parameter β with $\mu = k\sin\beta$ and $\kappa = k\cos\beta$.

The force potential U is then obtained based on the simulated pressure p and velocity fields $\mathbf{v}$ [2], i.e.,

$$U = (\pi a^3/3)[f_1|p|^2/(\rho_0 c_0^2) - (3/2)f_2\rho_0|\mathbf{v}|^2], \tag{2}$$

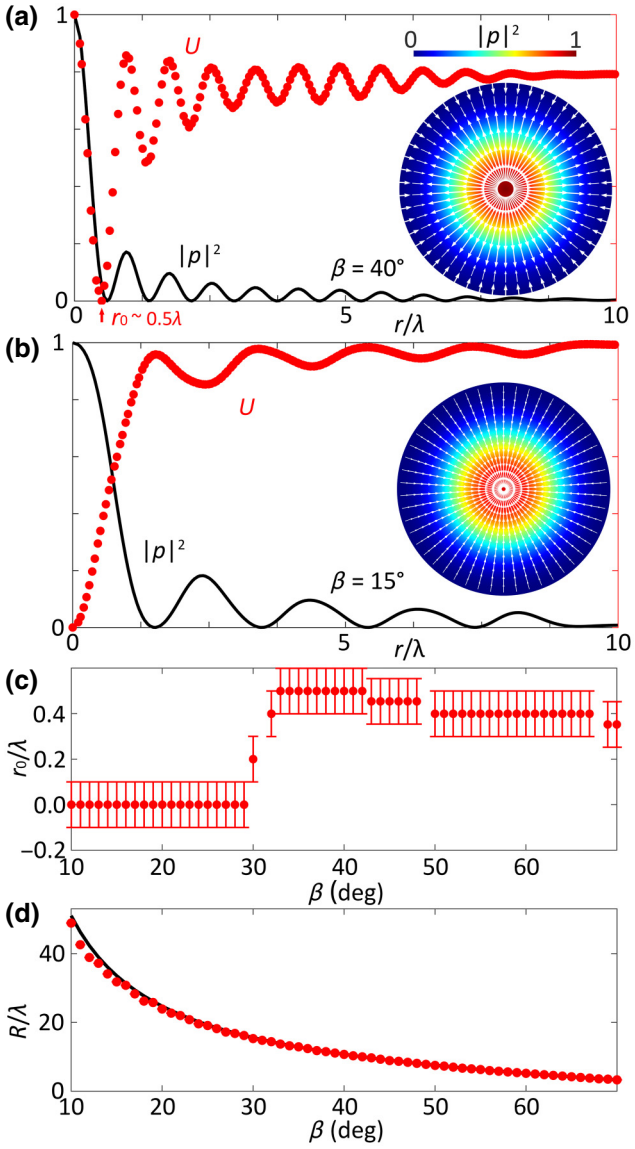

FIG. 2. Reversal of transverse particle trapping behaviors when reducing the angle from (a) $\beta = 40^\circ$ to (b) $\beta = 15^\circ$. Black solid lines: normalized squared pressure, $|p|^2$, at $z = 3\lambda$; red dots: normalized force potential U computed from Eq. (2) based on the simulated pressure and velocity fields. Insets: two-dimensional normalized squared pressure (color plots) and the corresponding radiation forces (white arrows). (c) Variation of the first trapping location r_0 near the beam axis. Transition angle occurs at $\beta \sim 29^\circ$. (d) Spatial range R for approximated Bessel beams from a finite sound source. Red dots: simulated results obtained based on the -3-dB location in the z direction; black line: curve fitting, $R \approx 0.9H/\tan\beta$ with H being the half-length of the finite source.

where a is the radius of the object, ρ_0 and c_0 are the mass density and the speed of sound of the background medium, and f_1 and f_2 are the monopole and dipole factors depending on the mass density ratio and bulk modulus ratio between the object and the surrounding medium [15].

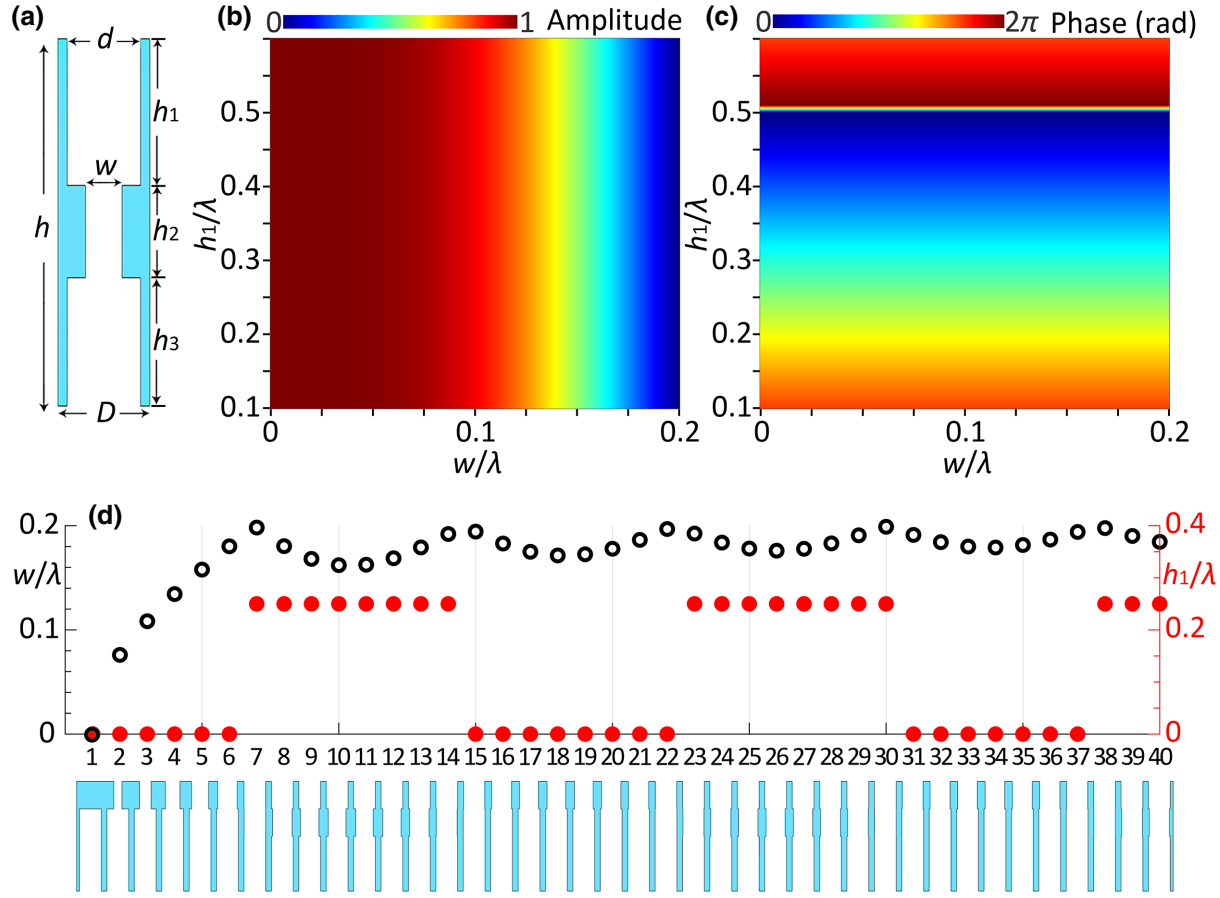

FIG. 3. (a) Illustration of one element of the artificial structure. Parameters are chosen as $h = \lambda$, $D = 0.25\lambda$, $d = 0.8D$, $h_2 = 0.5\lambda$, and $h = h_1 + h_2 + h_3$. The wavelength is λ. By adjusting the geometry parameters w and h_1, (b) the amplitude and (c) the phase of the reflected field can be modulated separately [Eq. (4)]. (d) The artificial structure used in the simulation for $\beta = 15^\circ$, and the corresponding geometry parameters w (black circles) and h_1 (red circles) for the 40 elements.

Here, rigid particles with $f_1 = 1 = f_2$ are used in the calculation since, for most solid objects, the density and bulk modulus are much larger than those of the background medium, air, so the results here are applicable to most elastic objects.

We first simulate the sound field of a finite zero-order Bessel beam with $\beta = 40^\circ$ [see Fig. 2(a)]. The red dots show the variation of the force potential [2] U [Eq. (2)] along the transverse location r/λ, with λ being the wavelength, and the black solid line shows the corresponding sound pressure. Particles are trapped to the local potential minimum; hence, for this case, a rigid particle cannot be trapped to the pressure maximum at the beam center ($r = 0$), which agrees with the previous conclusion from standing fields [2]. In addition, we find that for the off-axis transverse locations ($r > 0$), the force potential minimum coincides with the corresponding pressure minimum (or at most with a slight shift), where the particles can be trapped. In particular, the nearest trapping location to the beam center for this case is at $r_0 \sim 0.5\lambda$, which is useful for trapping particles [see the inset of Fig. 2(a) for the two-dimensional pressure profile (color plot) and the radiation forces computed based on the force potential, i.e., $\mathbf{F} = -\nabla U$ (white arrows)]. However, when the angle β is reduced to, for example, 15° [see Fig. 2(b)], the trapping behavior becomes different. Rigid particles are instead trapped to the central pressure maximum (see white arrows in the inset for the radiation force), and in addition, almost all the potential minimum along the transverse location corresponds to the pressure maximum, where the rigid particle can be trapped. Comparing Figs. 2(a) and 2(b), one can find that for a large β [2(a)], there exist more potential minima at the same transverse distance, so the spatial resolution for the trapping is improved. In addition, the transverse radiation force for a large β would be larger due to the large gradient of the force potential.

Here, the simulations are conducted with a two-dimensional axisymmetric model using the commercial software COMSOL Multiphysics. The size of the computation domain is 10λ in radius and 50λ in the z direction. Radiation boundaries are used to eliminate reflection. Maximum mesh size is set to be $\lambda/10$ to obtain precise and

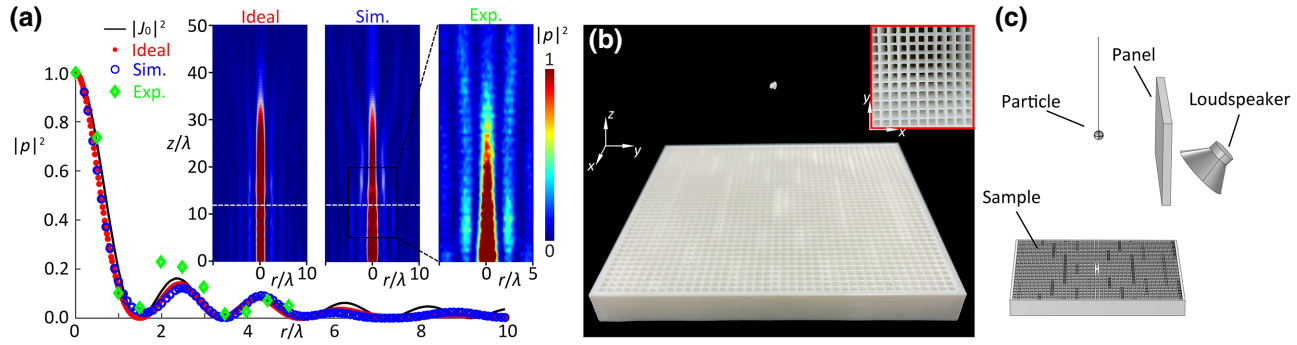

FIG. 4. Particle manipulations using finite Bessel beams. (a) Measured and simulated fields generated by the metastructure with the results compared with those for an ideal continuous distributed source. Comparison of the field profile $|p|^2$ at $z = 12\lambda$ (white dashed lines). J_0 is the zero-order Bessel function. (b) Photo of the transverse particle trapping experiment using acoustic metamaterials, where a foam ball is trapped at the center of the Bessel beam. The size of the sample is $20 \times 20 \times 2$ cm^3, and the diameter of the foam ball is approximately 2 mm. Inset: enlarged photo of the sample. (c) Illustration of the experimental setup.

accurate sound fields. The source is located at $z = 0$ and the background medium is air with a density of 1.21 kg/m^3 and speed of sound of 343 m/s.

We numerically observe the reversal of the transverse trapping behaviors for rigid particles on the central beam axis ($r = 0$) as the angle β is reduced, which recovers the previous theoretical prediction for ideal Bessel beams [15]. In order to examine the exact transition angle β for finite Bessel beams, a series of simulations are conducted for β from 10° to 70°. The nearest trapping location to the beam center is examined as a function of β [see Fig. 2(c)]. From the results, the trapping location first increases and then decreases as the angle β increases. The transition angle happens around $\beta \sim 29°$, agreeing with the predicted value $\beta \sim 28°$ in Fan and Zhang [15] within tolerance. The explanation of the reversal is interpreted by the contribution of axial velocity to the force potential and by momentum projection therein.

Like plane waves, an ideal Bessel beam cannot be created since it requires an infinitely large source and also an infinite amount of energy. Hence, the approximated Bessel beams only exist within a certain spatial range. We examine the relationship between the approximated spatial range R and the angle β [see red dots in Fig. 2(d)], where the spatial range R for each angle β takes the location of -3 dB along the propagating z direction. The relation between the spatial range R and the angle β for a finite source is

$$R \approx 0.9H / \tan\beta, \tag{3}$$

with H being the half-length of the source. Based on Eq. (3), the field can be approximately considered as a Bessel field within the allowable spatial range R for a given β and a source size H, and the Bessel beam with a small β could trap particles from a relatively long distance from the source.

III. EXPERIMENTAL REALIZATION

The desired acoustic Bessel beams can be generated using acoustic metamaterials. There are usually relatively complex couplings between the amplitude and the phase of the reproduced sound field by a sophisticated artificial structure, and the conventional phase-only modulated metamaterials generally ignore the error caused by the unavoidable amplitude variation. Hence, acoustic metamaterials with the ability to decouple the phase and amplitude modulations are preferred here.

In this work, a lossy acoustic metastructure is used to generate an acoustic Bessel beam with $\beta = 15°$ [see Fig. 3(a) for the cross section of one element in the structure] [36]. This structure can achieve the decoupled modulation of the amplitude A and the phase Φ [36], i.e.,

$$A = \frac{d^4 - w^4}{d^4 + w^4}, \quad \Phi = -\frac{4\pi h_1}{\lambda}. \tag{4}$$

The decoupled modulation of the amplitude and the phase allows for all the combinations in their full parameter ranges [that is, $A \in [0, 1]$ and $\Phi \in [0, 2\pi]$; see Figs. 3(b) and 3(c)], which is necessary to generate acoustic Bessel beams in our case. The viscosity effect of the metastructure here can be ignored since the boundary layer thickness is much smaller than the width of the elements [48,49]. The cross section of the structure and the corresponding geometry parameters w and h_1 for the 40 elements are shown in Fig. 3(d), which are used to generate a zero-order Bessel beam with $\beta = 15°$.

The measured and simulated fields $|p|^2$ generated via the acoustic metastructure are shown in Fig. 4(a). The results are further compared with the field generated by an ideal continuously distributed Bessel source of the same size. We examine the transverse profile of the field at $z = 12\lambda$ (white dashed lines). From the results, one can find that the fields generated via the acoustic metastructure (green

diamonds and blue circles) agree fairly well with the ideal source of the same size (red circles), and both of them follow the squared zero-order Bessel function (black solid line). Hence, with the aid of this structure, a zero-order Bessel beam is effectively generated and can be utilized for particle manipulations. As an example, the transverse particle trapping behavior for a small foam ball (diameter of approximately 2 mm) is examined and experimentally observed, where the particle is transversely trapped to the center of the field [see Fig. 4(b)]. Here, the sample of the metastructure is fabricated using a three dimension (3D) printer (Wiiboox Four) with the material polylactic acid (PLA). The printing resolution is 0.1 mm. A signal generator (RIGOL DG1032) and a power amplifier (CROWN XLi2500) are connected to a loudspeaker with a rated power of 100 W (Lutiane DL-630). The working frequency is 17 kHz, corresponding to a wavelength $\lambda \sim 2$ cm. The experimental diagram is shown in Fig. 4(c). The loudspeaker is fixed for a 45° incidence to the sample. An absorption panel is set at a specific position to separate incident and reflected acoustic fields. The acoustic fields are scanned in the target region with a step of 0.5 cm. Then an interpolation process is conducted on the measured data. To better investigate the transverse particle trapping, the foam is hung by a light string with a diameter of about 0.07 mm, and the particle can move freely in the transverse direction.

IV. CONCLUSION

In summary, we analyze both on-axis and off-axis particle trapping behaviors generated by finite acoustic axisymmetric Bessel beams. The reversal of the trapping behaviors on the beam axis is recovered when varying the paraxiality parameter β of the Bessel beam. In addition, the applicable spatial range for the approximated Bessel beam from a sound source of finite size is quantitatively investigated. A lossy acoustic metastructure is used for the generation of zero-order Bessel beams, which are then used to trap a small foam ball. Our work is beneficial to the further development of simplified acoustic tweezers using ordinary Bessel beams, which are desired for many applications involving particle manipulations.

ACKNOWLEDGMENTS

This work is supported by the National Natural Science Foundation of China (Grants No. 12204241 and No. 11974186), the Natural Science Foundation of Jiangsu Province (Grants No. BK20220924 and No. BK20200070), and the Open Research Foundation of Key Laboratory of Modern Acoustics, Ministry of Education, Nanjing University.

X.F. and Y.Z. contributed equally to this work.

[1] A. P. Sarvazyan, O. V. Rudenko, and W. L. Nyborg, Biomedical applications of radiation force of ultrasound: historical roots and physical basis, Ultrasound Med. Biol. **36**, 1379 (2010).

[2] L. P. Gor'kov, On the forces acting on a small particle in an acoustical field in an ideal fluid, Sov. Phys. Dokl. **6**, 773 (1962).

[3] J. Wu, Acoustical tweezers, J. Acoust. Soc. Am. **89**, 2140 (1991).

[4] P. L. Marston, Axial radiation force of a Bessel beam on a sphere and direction reversal of the force, J. Acoust. Soc. Am **120**, 3518 (2006).

[5] L. K. Zhang and P. L. Marston, Geometrical interpretation of negative radiation forces of acoustical Bessel beams on spheres, Phys. Rev. E **84**, 035601 (2011).

[6] L. K. Zhang and P. L. Marston, Axial radiation force exerted by general non-diffracting beams, J. Acoust. Soc. Am. **131**, EL329 (2012).

[7] S. Xu, C. Qiu, and Z. Liu, Transversally stable acoustic pulling force produced by two crossed plane waves, Europhys. Lett. **99**, 44003 (2012).

[8] C. R. P. Courtney, B. W. Drinkwater, C. E. M. Demore, S. Cochran, A. Grinenko, and P. D. Wilcox, Dexterous manipulation of microparticles using Bessel-function acoustic pressure fields, Appl. Phys. Lett. **102**, 123508 (2013).

[9] C. E. M. Démoré, P. M. Dahl, Z. Yang, P. Glynne-Jones, A. Melzer, S. Cochran, M. P. MacDonald, and G. C. Spalding, Acoustic Tractor Beam, Phys. Rev. Lett. **112**, 174302 (2014).

[10] A. Marzo, S. A. Seah, B. W. Drinkwater, D. R. Sahoo, B. Long, and S. Subramanian, Holographic acoustic elements for manipulation of levitated objects, Nat. Commun. **6**, 8661 (2015).

[11] K. Melde, A. G. Mark, T. Qiu, and P. Fischer, Holograms for acoustics, Nature **537**, 518 (2016).

[12] A. Marzo, A. Ghobrial, L. Cox, M. Caleap, A. Croxford, and B. W. Drinkwater, Realization of compact tractor beams using acoustic delay-lines, App. Phys. Lett. **110**, 014102 (2017).

[13] A. Marzo, M. Caleap, and B. W. Drinkwater, Acoustic Virtual Vortices with Tunable Orbital Angular Momentum for Trapping of Mie Particles, Phys. Rev. Lett. **120**, 044301 (2018).

[14] L. K. Zhang, Reversals of Orbital Angular Momentum Transfer and Radiation Torque, Phys. Rev. Appl. **10**, 034039 (2018).

[15] X. D. Fan and L. K. Zhang, Trapping Force of Acoustical Bessel Beams on a Sphere and Stable Tractor Beams, Phys. Rev. Appl. **11**, 014055 (2019).

[16] X.-D. Fan and L. Zhang, Phase shift approach for engineering desired radiation force: Acoustic pulling force example, J. Acoust. Soc. Am. **150**, 102 (2021).

[17] N. Korozlu, A. Biçer, D. Sayarcan, O. A. Kaya, and A. Cicek, Acoustic sorting of airborne particles by a phononic crystal waveguide, Ultrasonics **124**, 106777 (2022).

[18] D. B. Thiessen, L. K. Zhang, and P. L. Marston, Radiation force on spheres in helicoidal Bessel beams modeled using finite elements, J. Acoust. Soc. Am. **125**, 2552 (2009).

[19] D. Baresch, J. L. Thomas, and R. Marchiano, Three-dimensional acoustic radiation force on an arbitrarily located elastic sphere, J. Acoust. Soc. Am. **133**, 25 (2013).

[20] G. T. Silva, J. H. Lopes, and F. G. Mitri, Off-axial acoustic radiation force of repulsor and tractor Bessel beams on a sphere, IEEE Trans. Ultrason. Ferroelectr. Freq. Control **60**, 1207 (2013).
[21] Z. Liu, X. Zhang, Y. Mao, Y. Y. Zhu, Z. Yang, C. T. Chan, and P. Sheng, Locally resonant sonic materials, Science **289**, 1734 (2000).
[22] Y. Li, B. Liang, Z.-m. Gu, X.-y. Zou, and J.-c. Cheng, Reflected wavefront manipulation based on ultrathin planar acoustic metasurfaces, Sci. Rep. **3**, 1 (2013).
[23] J. Zhao, B. Li, Z. Chen, and C.-W. Qiu, Manipulating acoustic wavefront by inhomogeneous impedance and steerable extraordinary reflection, Sci. Rep. **3**, 1 (2013).
[24] P. Zhang, T. Li, J. Zhu, X. Zhu, S. Yang, Y. Wang, X. Yin, and X. Zhang, Generation of acoustic self-bending and bottle beams by phase engineering, Nat. Commun. **5**, 1 (2014).
[25] Y. Li, X. Jiang, R.-q. Li, B. Liang, X.-y. Zou, L.-l. Yin, and J.-c. Cheng, Experimental Realization of Full Control of Reflected Waves with Subwavelength Acoustic Metasurfaces, Phys. Rev. Appl. **2**, 064002 (2014).
[26] K. Tang, C. Qiu, M. Ke, J. Lu, Y. Ye, and Z. Liu, Anomalous refraction of airborne sound through ultrathin metasurfaces, Sci. Rep. **4**, 1 (2014).
[27] Y. Xie, W. Wang, H. Chen, A. Konneker, B.-I. Popa, and S. A. Cummer, Wavefront modulation and subwavelength diffractive acoustics with an acoustic metasurface, Nat. Commun. **5**, 1 (2014).
[28] Y. Li, X. Jiang, B. Liang, J.-c. Cheng, and L. Zhang, Metascreen-Based Acoustic Passive Phased Array, Phys. Rev. Appl. **4**, 024003 (2015).
[29] G. Ma and P. Sheng, Acoustic metamaterials: From local resonances to broad horizons, Sci. Adv. **2**, e1501595 (2016).
[30] S. A. Cummer, J. Christensen, and A. Alù, Controlling sound with acoustic metamaterials, Nat. Rev. Mater. **1**, 1 (2016).
[31] X. Zhu, K. Li, P. Zhang, J. Zhu, J. Zhang, C. Tian, and S. Liu, Implementation of dispersion-free slow acoustic wave propagation and phase engineering with helical-structured metamaterials, Nat. Commun. **7**, 1 (2016).
[32] X. Jiang, Y. Li, B. Liang, J.-c. Cheng, and L. Zhang, Convert Acoustic Resonances to Orbital Angular Momentum, Phys. Rev. Lett. **117**, 034301 (2016).
[33] X.-D. Fan, Y.-F. Zhu, B. Liang, J. Yang, and J.-C. Cheng, Broadband convergence of acoustic energy with binary reflected phases on planar surface, Appl. Phys. Lett. **109**, 243501 (2016).
[34] Y. Zhu, X. Fan, B. Liang, J. Cheng, and Y. Jing, Ultrathin acoustic metasurface-based Schroeder diffuser, Phys. Rev. X **7**, 021034 (2017).
[35] Y. Li, C. Shen, Y. Xie, J. Li, W. Wang, S. A. Cummer, and Y. Jing, Tunable Asymmetric Transmission via Lossy Acoustic Metasurfaces, Phys. Rev. Lett. **119**, 035501 (2017).
[36] Y. Zhu, J. Hu, X. Fan, J. Yang, B. Liang, X. Zhu, and J. Cheng, Fine manipulation of sound via lossy metamaterials with independent and arbitrary reflection amplitude and phase, Nat. Commun. **9**, 1 (2018).
[37] B. Assouar, B. Liang, Y. Wu, Y. Li, J.-C. Cheng, and Y. Jing, Acoustic metasurfaces, Nat. Rev. Mater. **3**, 460 (2018).
[38] X.-D. Fan, B. Liang, J. Yang, and J.-C. Cheng, Illusion for airborne sound source by a closed layer with subwavelength thickness, Sci. Rep. **9**, 1 (2019).
[39] X.-D. Fan and L. Zhang, Acoustic orbital angular momentum hall effect and realization using a metasurface, Phys. Rev. Res. **3**, 013251 (2021).
[40] S. Zhang, C. Xia, and N. Fang, Broadband Acoustic Cloak for Ultrasound Waves, Phys. Rev. Lett. **106**, 024301 (2011).
[41] X. Zhu, B. Liang, W. Kan, X. Zou, and J. Cheng, Acoustic Cloaking by a Superlens with Single-Negative Materials, Phys. Rev. Lett. **106**, 014301 (2011).
[42] X. Jiang, B. Liang, X.-y. Zou, L.-l. Yin, and J.-c. Cheng, Broadband field rotator based on acoustic metamaterials, Appl. Phys. Lett. **104**, 083510 (2014).
[43] W. Kan, B. Liang, R. Li, X. Jiang, X.-y. Zou, L.-l. Yin, and J. Cheng, Three-dimensional broadband acoustic illusion cloak for sound-hard boundaries of curved geometry, Sci. Rep. **6**, 1 (2016).
[44] H. Gao, Y.-f. Zhu, X.-d. Fan, B. Liang, J. Yang, and J.-C. Cheng, Non-blind acoustic invisibility by dual layers of homogeneous single-negative media, Sci. Rep. **7**, 1 (2017).
[45] S. Inoue, S. Mogami, T. Ichiyama, A. Noda, Y. Makino, and H. Shinoda, Acoustical boundary hologram for macroscopic rigid-body levitation, J. Acoust. Soc. Am. **145**, 328 (2019).
[46] Y. Zhu and B. Assouar, Systematic design of multiplexed-acoustic-metasurface hologram with simultaneous amplitude and phase modulations, Phys. Rev. Mater. **3**, 045201 (2019).
[47] Y. Zhu, N. J. Gerard, X. Xia, G. C. Stevenson, L. Cao, S. Fan, C. M. Spadaccini, Y. Jing, and B. Assouar, Systematic design and experimental demonstration of transmission-type multiplexed acoustic metaholograms, Adv. Funct. Mater. **31**, 2101947 (2021).
[48] G. Ward, R. Lovelock, A. Murray, A. P. Hibbins, J. R. Sambles, and J. Smith, Boundary-Layer Effects on Acoustic Transmission Through Narrow Slit Cavities, Phys. Rev. Lett. **115**, 044302 (2015).
[49] M. Molerón, M. Serra-Garcia, and C. Daraio, Visco-thermal effects in acoustic metamaterials: From total transmission to total reflection and high absorption, New J. Phys. **18**, 033003 (2016).